Accepted Manuscript

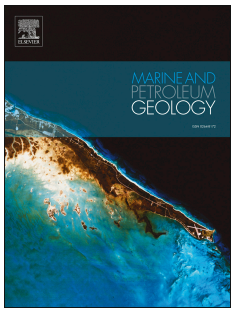

Diagenetic history and reservoir properties of the Cenomanian-Turonian carbonates in southwestern Iran and the Persian Gulf

E. Hajikazemi, I.S. Al-Aasm, M. Coniglio

PII: S0264-8172(17)30242-8

DOI: 10.1016/j.marpetgeo.2017.06.035

Reference: JMPG 2969

To appear in: *Marine and Petroleum Geology*

Received Date: 29 March 2016

Revised Date: 19 December 2016

Accepted Date: 21 June 2017

Please cite this article as: Hajikazemi, E., Al-Aasm, I.S., Coniglio, M., Diagenetic history and reservoir properties of the Cenomanian-Turonian carbonates in southwestern Iran and the Persian Gulf, *Marine and Petroleum Geology* (2017), doi: 10.1016/j.marpetgeo.2017.06.035.

DIAGENETIC HISTORY AND RESERVOIR PROPERTIES OF THE CENOMANIAN-TURONIAN CARBONATES IN SOUTHWESTERN IRAN AND THE PERSIAN GULF

E. Hajikazemi[1*], I.S. Al-Aasm[2], M. Coniglio[3]

1. Iranian Offshore Oil Company, Tehran, Iran.

2. Department of Earth and Environmental Sciences, University of Windsor, Windsor, Ontario, N9B 3P4 Canada.

3. Department of Earth and Environmental Sciences, University of Waterloo, Waterloo, Ontario N2L 3G1, Canada.

**author for correspondence, e-mail: ekazemi@iooc.co.ir*

ABSTRACT

Shallow-marine carbonates of the mid-Cretaceous Sarvak Formation are important reservoir rocks in southern Iran and the Persian Gulf region. These carbonates were deposited on the margin of the Arabian Plate and rest on the Kazhdumi Formation, which is one of the major hydrocarbon source rocks in the region. The top of the Sarvak Formation coincides with the regional Turonian unconformity. Most of the observed diagenetic features are genetically related to meteoric waters entering the Sarvak Formation during Cenomanian-Turonian and mid-Turonian uplift and the subsequent paleoexposure.

Integration of field and petrographic studies and isotope geochemistry reveals the history of a variety of diagenetic processes, which include dissolution and development of secondary porosity which enhance reservoir properties of the Upper Sarvak carbonates. Various types of calcite cements were identified as the main cause for porosity loss in these carbonates. Their diagenetic environment is discussed using the geochemical data acquired as part of the present study.

The $\delta^{18}O$ and $\delta^{13}C$ values (-12.3 to -0.6 ‰ and -5.8 to 3.6‰ VPDB, respectively) of the cements indicate precipitation from marine, meteoric and/or mixed meteoric-marine fluids. Some drusy calcite cements exhibit $\delta^{18}O$ and $\delta^{13}C$ values (-5.1 and 0.8

‰ VPDB, respectively) and higher $^{87}Sr/^{86}Sr$ ratios, comparing to mid-Cretaceous carbonates, (i.e., 0.70747), which may indicate precipitation from meteoric waters. Lower $\delta^{18}O$ and $\delta^{13}C$ values (e.g. -5.1, 0.8‰ VPDB) combined with higher $^{87}Sr/^{86}Sr$ ratios (e.g., 0.70747) of some drusy calcite could confirm their precipitation from meteoric waters.

Lower $\delta^{18}O$ values of some blocky calcite cements (e.g., -12.3 ‰ VPDB) and matrix-replacive compression-related dolomites (i.e., -7.3 to -3.4‰ VPDB) suggest their precipitation at rising temperatures during burial.

The range of $\delta^{13}C$ values (-5.8 to 3.6 ‰ VPDB) suggests that the main source of carbon in the calcite cements was primarily marine mixed with isotopically more negative carbon from atmospheric/soil-derived CO_2.

Keywords: Cenomanian-Turonian, Sarvak Formation, Iran, unconformity, carbonate diagenesis, stable isotopes

INTRODUCTION

The Sarvak Formation, the most prolific regional oil reservoir after the Asmari Formation, was deposited during the Cenomanian- Early Turonian on a carbonate platform located on the passive margin of the Arabian Plate (Setudehnia, 1978; Ziegler, 2001). It mainly consists of shallow water carbonates.

The reservoir zone of these carbonates is located in the upper part of the succession and usually characterized by rudist-foraminifera bioherms (Motiei, 1993; Hajikazemi*et al*., 2010; Piryaei*et al*., 2010).The formation is bounded on top by the regional Turonian unconformity, which is associated with widespread meteoric diagenesis (Hajikazemi *et al*., 2010). Multiple subaerial exposures of the Sarvak Formation during the Cenomanian-Turonian also caused development of extensive secondary porosity and permeability (Hajikazemi*et al*., 2010). The relationship between the depositional facies, their preservation and creation of porosity has been outlined by Hollis (2011). In spite of previous studies of the Sarvak Formation (e.g., Taghavi *et al*., 2006; Hajikazemi *et al*., 2002, 2010, 2012; Sharp *et al*., 2010; Hollis, 2011; Vincent et al., 2015), due to their heterogeneity and complexity, the detailed

diagenetic history of the Sarvak carbonates in southern Iran remains unclear and warrants further investigations. In addition, little is known about geochemical characteristics and evolution of the diagenetic fluids.

This paper presents the results of a detail diagenetic study of the Sarvak Formation based on data from different localities in southwestern Iran and the Persian Gulf. These include the type section at Bangestan Mountain and Shahneshin Mountain in Fars province, core samples from Rag-e Sefid and Bibi Hakimeh oilfields in southwestern Iran and also the Sirri offshore oilfield in the Persian Gulf (Fig.1). These sites were sampled and studied utilizing petrographic, trace element and stable isotope analyses, in order to evaluate the controls on reservoir characteristics.

Regional Geological Setting

During the mid-Cretaceous, the northeastern margin of the Arabian Plate was occupied by a platform characterized by substantial local variations in accommodation space creation and depositional environments. Thickness and facies variations of the Sarvak carbonates has been documented in southwestern Iran in many studies (e.g. Setudenia 1978 and Hajikazemi et al., 2010).These remarkable variations were mainly caused by relative sea level changes controlled by a combination of eustacy, local tectonics and salt movement during Cenomanian-Turonian (Videtich *et al*., 1988; Farzadi and Hesthmer, 2007; Piryaei *et al*., 2010, 2011; Vincent et al., 2015). Sedimentation rates varied considerably as indicated by isopach maps of the mid-Cretaceous time (Koop and Stoneley, 1982; Ghazban, 2007). Ghazban, 2007, suggesting local tectonic instability caused by salt tectonics and extensive uplift and erosion.The presence of basement highs also influenced basin configurations and sedimentation locally (Taghavi *et al*., 2006; Hajikazemi *et al*., 2010).

The Late Cenomanian was marked by the initiation of tectonic activity associated with the ongoing continental collision taking place in the region at this time. The Cenomanian-Campanian abduction of ocean crust along the southeastern and eastern margins of the Arabian plate caused re-activation of deep-seated regional faults and displacement of the Hormuz salt (Ghazban, 2007) which initiated episodes of regional uplift and erosion of the upper part of the Sarvak succession in the studied area.

Exposure features, varying from incipient microkarst to epikarst and deep channel incision, have been reported (see Droste, 2010; Hollis, 2011, Hajikazemi et al., 2010). Two main unconformities have been recognized in southern Iran and the Persian Gulf: a regional Turonian unconformity and a more local Cenomanian-Turonian break (Taghavi *et al*., 2006; Beiranvand *et al*., 2007; Hajikazemi *et al*., 2010). These unconformities are characterized by karstification, dissolution breccia and development of paleosols (Hajikazemi et al., 2010; 2012; Sharp *et al*., 2010).
"The two unconformities display evidence of deep erosion and truncation of the underlying formations (Hajikazemi et al., 2010; 2012). Similar unconformities have been described in United Arab Emirates, Qatar and Khuzestan area (Harris and Frost, 1984; Van Buchem, 2006; Hollis, 2011).

Stratigraphy and Depositional Environment

At the type section, the Sarvak Formation consists of several different carbonate facies with a total thickness of 821 m (Motiei, 1993). The formation conformably overlies the Kazhdumi Formation and is unconformably overlain by the marls of the Gurpi Formation of Maastrichtian age (Fig.2).

The lower part of the formation is composed of argillaceous micritic limestone and thin beds of marl. The middle portion consists of massive chalky limestones with iron-rich siliceous nodules and rudist fragments. The upper part comprises massive limestones with the top most strata consisting of weathered, brecciated and ferruginous limestone. The unconformity at the top of the Sarvak Formation is marked by pedogenesis, brecciation, karstification, hematite and Fe/Mn nodule development (Hajikazemi et al., 2010; Mehrabi et al., 2015; Vincent et al., 2015).

These carbonates were deposited on a low- angled platform on the margins of an intrashelf basin. The shallowing-upwards carbonates of the Sarvak Formation are composed of Oligostegina wackestone, bioclastic wacke/packstone, rudist floatstone, rudist grainstone, benthic foraminifera wacke/packestone, representing four main depositional environments of a ramp setting (i.e. inner-ramp, mid-ramp, outer-ramp and open marine or basinal (Taghavi*et al*., 2006; Hajikazemi*et al*., 2010). Sedimentary features such as burrows and geopetal fabrics dominate the inner-ramp

setting the inner-ramp setting. Mid-ramp facies are mainly restricted to the Upper Sarvak Formation whereas outer-ramp facies occur in the Lower Sarvak Formation. Basinal facies which consist mainly of *Oligostegina* wackestone/packstone susually occur in the lower Sarvak Formation. Further description of sedimentary facies and their environmental interpretation can be found in Hajikazemi *et al*., 2010, Esrafili-Dizaji, *et al.*, 2015 and Vincent *et al*., 2015.

MATERIALS AND METHODS

The carbonate units from the surface and core sections were logged and sampled based on observed facies and/or diagenetic variations. Petrographic thin sections from both outcrop sections and cores were examined using transmitted light (see figure 1 for locality of sampling).Cathodoluminescence microscopy of over 100 representative samples mainly from upper part of the Sarvak carbonates which usually shows reservoir properties and contain different type of calcite cements and dolomite,was performed using a Technosyn 8200 MKII model cold cathodoluminescence stage with a 12-15 kv beam and a current intensity of 420-430 μA on the unstained halves of the uncovered thin sections. Core samples were impregnated with an epoxy mixed with blue dye for porosity identification.

Calcite cements, dolomites and their host calcite matrix were micro-sampled using a microscope-mounted dental drill assembly. Powdered samples were reacted with 100% pure phosphoric acid at 25°C for calcite and 50°C for dolomite for 4 hours (Al-Aasm *et al*., 1990) and the evolved CO_2 gas was analyzed for stable oxygen and carbon isotopes utilising a Finnigan Mat Delta-Plus mass spectrometer.All analyses for oxygen and carbon isotopes are reported in per mil (‰) notation relative to the Vienna Pee Dee Belemnite (VPDB) standard. Replicate analyses using these procedures and comparisons with laboratory standards, give a precision better than 0.05‰ for both $\delta^{18}O$ and $\delta^{13}C$ values.

Major and trace element data were obtained using an ICP-MS at the Great Lake Environmental Research Institute at the University of Windsor. Each sample was weighed, reacted with 2 grams of 5% HNO_3 and diluted with 3 millilitres of twice-distilled water. Calibration of the ICP-MS was achieved using reference materials and

a procedural blank selected to cover the range of elemental concentrations expected in samples. Data are reported as weight percent.

DIAGENETIC FEATURES AND RESERVOIR CHARACTERISTICS

A variety of diagenetic features were recognized in the Sarvak carbonates. Calcite was the most abundant pore-filling cement. Other diagenetic constituents include dolomite and minor pyrite. A paragenetic sequence is presented in Figure3 based on standard petrographic and CL observations and geochemical considerations. The timing of diagenetic events was determined mainly from observed textural relationships and to a lesser extent on the results of geochemical analysis. Diagenetic events, which influenced the reservoir characteristics of these carbonates, include dissolution, compaction, recrystallization, fracturing, dolomitization, pyrite formation and calcite cementation. Dissolution and dolomitization are the most porosity-enhancing diagenetic features in reservoir units. The major events are discussed in turn below.

Pyrite Formation

Two types of pyrite were observed in the Sarvak Formation:(1) microcrystalline framboidal pyrite, which is common below the unconformity surface(s); and (2) coarse crystalline pyrite which is more abundant in subsurface samples. Neither type of pyrite is widespread. Framboidal pyrite consists of numerous spheroidal clusters of small, discrete, equant microcrystals (Fig. 4a). Coarse crystalline pyrite occurs as euhedral crystals, which replace the calcite matrix or partially fill fractures, suggesting formation during later diagenesis. Their occurrence reduces the porosity of some fractures (Fig. 4b).

Calcite Cementation

Five types of calcite cement were observed in the Sarvak carbonates:

1. Fine crystalline isopachous rim –cements(rare), surrounding some skeletal grains in grainstone/ packstons;
2. Fine to medium crystalline equant calcite cement, filling interparticle pores in packstonesand grainstones (Fig. 4c);
3. Syntaxial overgrowth calcite (rare), surrounding echinoid fragments in grainstones;

4. Drusy mosaic calcite, filling fractures, vugs and molds (Fig.4d); and
5. Coarse blocky sparry calcite, partially filling the remaining voids in some fractures and the body cavities of rudists and vugs (Fig. 4e,f).

The cement types were distinguished by their petrographic characteristicsand also their response to cathodoluminescence. Isopachous rim- cements and syntaxial overgrowth calcite cements are generally non-luminescent. Equant calcite cements consist of dark to non-luminescent crystals with thin, brightly luminescent rims (Fig. 5a, b). Drusy mosaic calcite cement is composed of alternating dull to non-luminescent and bright orange-to-yellow highly luminescent bands.

Coarse blocky calcite was the latest cement phase, which partially or completely fills some vugs, resulting in porosity reduction and consequently affects the reservoir quality.This calcite phase is commonly ferroan and characterized by dull to non-luminescent crystals (Fig. 5a, b). In core samples, this type of cement also appears along some stylolites with two- phase fluid inclusions in some of the larger crystals.
The presence of two-phase fluid inclusions and cross-cutting relationships confirm that they must be a component of later precipitation of cement under higher ambient temperatures compared to earlier cements. It is important to note that an apparent consistency in the temperatures of cementation across the region with homogenization temperatures above 80^{o}C has also been reported by other researchers (see Videtich *et al*., 1988; Sharp *et al*., 2010).

Drusy mosaic and blocky calcite cements are volumetrically the most important calcite cements. These cements were selected for geochemical analyses because they could be sampled relatively easily without contamination by surrounding matrix. Obtaining samples from earlier cement types was not possible due to their small volume and crystal size.

Dissolution

Vuggy and moldic porosity are the dominant secondary porosity type; particularly in the Upper Sarvak Formation. Based on petrographic observations, log data and porosity measurements of core samples, porosity ranges from 5 to over 25 percent in some intervals.

In core specimen and surface sections, vugs are up to a few centimetres in dimension. Cavernous (man-size) porosity is present below the unconformity surface(s), especially in Shahneshin Mountain surface section (Fig. 6a). Some of the molds and vugs may be totally or partially filled with calcite cement or bitumen (Fig. 6b). However, many of them remain open (Fig.6c).

Mechanical and Chemical Compaction

Mechanical and chemical compaction has influenced the reservoir characteristics in the Sarvak Formation carbonates. Evidence for compactional modification is ubiquitous in the formation (Asghari and Adabi, 2014; Hollis, 2011). Mechanical compaction caused porosity reduction by fusing and/or breakage of the grains and decreasing the interparticle porosity in packstones. Dissolution seams and stylolites are the most common chemical compaction features, especially in mud-supported rock units (Fig. 5d).

Recrystallization

Partial recrystallization of the calcite matrix and bioclasts was observed in some intervals, especially below the unconformity surface(s), and also adjacent to some stylolites. Recrystallization reduced primary matrix porosity by forming larger crystals with a tight texture and no/less intercrystalline pore space in between.

Fracturing

Fractures, observed in subsurface samples and in larger scale in outcrops, constitute an important type of secondary porosity, particularly in the Upper Sarvak Formation. Fracture orientations vary from vertical to horizontal, and widths range from hairline up to a few centimetres across. The fractures are grouped into two main sets. The oldest set is predominant and includes vertical to sub-vertical fractures. These fractures have the apertures greater than 2 mm in some core samples and up to few centimetres in surface sections. These individual fractures are partially or completely filled with calcite cement .The second set is horizontal to sub- horizontal fractures. They cross-cut the earlier set; their apertures are not wide open (few micrometers in most samples)and most are devoid of any cementation. This second set of fractures cross cuts stylolites and dissolution seams (Fig.5e).

Dolomitization

Dolomite is uncommon in the studied wells and outcrops of the upper part of the Sarvak Formation, and when present constitutes less than 10% of the matrix.

Three types of dolomite were observed in studied sections:

Dolomite I: finely crystalline dolomite cement (up to 20 μm in size) filling interparticle porosity in brecciated intervals underlying the unconformity surface (s); Dolomite II: subhedral- euhedral fine to medium-crystalline (40-60 μm) clear dolomite, replacing carbonate matrix in association with dissolution seams; and Dolomite III: euhedral, medium-crystalline, cloudy-centred clear-rimmed dolomite with crystal size reaching to 70 μm or greater. This type of dolomite partially replaces calcite matrix adjacent to stylolites in some argillaceous intervals. The latest generation of dolomite (i.e., Dolomite III), which commonly observed in core samples, creates intercrystalline porosity. Live oil fills the porosity between dolomite crystals (Fig. 5f). The intervals containing Dolomite III with the porosity over 15 percent usually form good quality reservoir units in studied oilfields and elsewhere in the area. Only the latest dolomites (Dolomite III) were sufficiently abundant to be sampled for carbon and oxygen stable isotope analysis.

Palaeosol Formation

The upper part of the Sarvak Formation in outcrops and some subsurface sections (e.g. Sirri oil field) is composed of exposure-related features and products including palaeosols in the shape of bauxite and laterite or a mixture of ferroan pisoids and quartz grains in a clay matrix.

ISOTOPE GEOCHEMISTRYAND ELEMENTAL ANALYSES

The $\delta^{13}C$ and $\delta^{18}O$ values and the $^{87}Sr/^{86}Sr$ ratios in addition to concentrations of Ca, Mg, Mn and Sr, were determined in rudist shells, matrix material (i.e. micrite) and cement to determine diagenetic conditions in which the cements were precipitated.

Calcite Matrix

The $\delta^{13}C$ and $\delta^{18}O$ values for the samples analyzed are summarized in Tables 1, 2.1 and 2.2 and illustrated in Figure (7).The $\delta^{13}C$ and $\delta^{18}O$ values of the calcite matrix range from -6.4 to +4.1‰ VPDB and -9.4 to -0.9‰ VPDB, respectively. Most of the $\delta^{13}C$ values from the Sarvak Formation (except the values obtained from the samples taken below the paleoexposure surfaces) are typical of Cenomanian-Turonian carbonates deposited in warm-water conditions in low latitudes (see Veizer *et al*., 1999 for values) and are compatible with the values obtained by other workers for this

time interval (Immenhauser *et al.,* 2005; Steuber, 1996; Arthur, *et al*., 1988; Scholle and Arthur, 1980).

Rudist Shells

Nineteen samples of rudist shells from cores and surface sections were analyzed for $\delta^{13}C$, $\delta^{18}O$, and $^{87}Sr/^{86}Sr$ and major and trace element contents (Table 2.2). Rudist shells can potentially record marine water chemistry at the time they formed, because their outer layers originally consisted of diagenetically stable low-Mg calcite (Al-Aasm and Veizer, 1986b). Based on their CL characteristics, the rudist shells have not been affected by later alteration and their isotopic values could be used as reference to compare other carbonate phases.

The $\delta^{13}C$ and $\delta^{18}O$ values of the rudist shells range from 1.3 to 2.7‰ and -5.6 to -3.0‰ VPDB, respectively.

Calcite Cements

Drusy mosaic calcite cements have $\delta^{13}C$ and $\delta^{18}O$ values ranging from -5.8 ‰ to +3.6‰ and -9.3‰ to -0.6‰ VPDB, respectively. The $\delta^{13}C$ and $\delta^{18}O$ values for blocky calcite cement ranged from -2.4 to 3.6‰ and from -12.3 to -2.8‰, respectively (Fig. 8). Calcite cements show a wider range of $\delta^{18}O$ values compared to matrix material. Some blocky calcite cements have more negative $\delta^{18}O$ values compared to matrix and drusy mosaic cements and their $\delta^{13}C$ values show a significant overlap with other carbonate components.

On a plot of $\delta^{13}C$ versus $\delta^{18}O$, blocky calcite cements sampled from vugs and fractures fall into three distinct groups (Fig. 9). Group 1, comprising six samples of blocky calcite cement, shows the most negative values for and $\delta^{18}O$ and $\delta^{13}C$ (-12.3, -5.4 ‰ and -2.4 and +0.3 ‰VPDB respectively). Group 2 exhibits the most positive values ($\delta^{18}O$ between -3.8, -3.5‰ and $\delta^{13}C$ between +2.4 and +3.5‰ VPDB), which are compatible with mid-Cretaceous marine carbonates. Group 3 contains the largest number of samples whose $\delta^{13}C$ and $\delta^{18}O$ have relatively narrow ranges of values ($\delta^{18}O$ between -6.7, -4.2‰ and $\delta^{13}C$ between +1.2 and +2.8‰VPDB).

Dolomite

Nine samples of dolomite III, the most abundant type of dolomite in the Upper Sarvak Formation in the studied wells, were analyzed for stable carbon and oxygen isotopes.

The $\delta^{13}C$ values ranges from 1.5 to 5.0‰ VPDB and $\delta^{18}O$ ranges from -7.3 to -3.4‰ VPDB (Table 1). A plot of $\delta^{13}C$ vs. $\delta^{18}O$ for these dolomites is presented in Figure 10.

Palaeosol

Five samples of palaeosol from below the unconformity surface in the Shahneshin Mountain surface section were analyzed for $\delta^{13}C$ and $\delta^{18}O$ values. They range from -5.7 to -2.9 ‰ VPDB and -6.1 to -4.2‰ VPDB, respectively (Table 1).

DISCUSSION

Diagenesis of depositional components

Diagenetic processes in carbonates generally produce phases with depleted $\delta^{13}C$ and $\delta^{18}O$ while preserved marine carbonates display positive$\delta^{13}C$ and $\delta^{18}O$ (Veizer et al., 1999).

The most positive $\delta^{13}C$ and $\delta^{18}O$ values were measured in the non-luminescent rudist shells which considered to be the most pristine values and used as reference values for comparison with other carbonate phases. The range of $\delta^{13}C$ values is similar to recorded ranges of mid-Cretaceous marine carbonates (e.g., Veizer *et al*., 1999). Small variations in $\delta^{13}C$ values most likely reflect original differences in terms of the oxidation of organic matter incorporated into the marine carbonates during their precipitation.

With eustatic sea level changes during the mid-Cretaceous, the $\delta^{13}C$ also fluctuated in the same manner, and consequently the variations in $\delta^{13}C$ values from analysed matrix samples could be an indication of eustatic sea-level changes (see Jenkyns, 1994; Hajikazemi *et al.,* 2012). Such shifts in $\delta^{13}C$ values have also been illustrated in studied sections of the Sarvak carbonates in other areas within southern Iran (Vincent *et al*., 2015). Therefore, we conclude that the $\delta^{13}C$of the Sarvak carbonates can be utilized as a constraining tool for stratigraphic correlation (see Hajikazemi et al., 2012).

The $\delta^{18}O$ signature of the majority of the samples obtained from low Mg-calcite matrix represents original sea water signature. Based on cathodoluminescence petrography, most of the calcite matrix diagenetically remained unaltered except those sampled immediately below the unconformity surfaces (see Hajikazemi *et al*., 2010; 2012).

Calcite matrix below the paleoexposure surfaces with depleted $\delta^{13}C$ and $\delta^{18}O$ values are often luminescent, activated by Mn (Marshall, 1992; Savard et al., 1995) show diagenetic alteration under the influence of meteoric waters. Considering Mn concentration as a proxy for alteration by meteoric water, a plot of $\delta^{18}O$ vs. Mn concentrations for majority of the samples would show no correlation, implying that they have not considerably been altered (Fig. 11). Furthermore, the low Mn values obtained from calcite matrix (2-40 ppm in the majority of measured samples in this study and 1 - 35 ppm in Asghari and Adabi, 2014) are also consistent with little or no diagenetic alteration.

Cement Diagenesis

Meteoric diagenesis is characterized by depleted $\delta^{13}C$and $\delta^{18}O$ values (James and Choquette, 1990) while burial diagenesis could modify only the original $\delta^{18}O$. The $\delta^{13}C$ values remain essentially unchanged by diagenesis in sediments with low organic carbon content (Barrera and Keller, 1990).

The more positive $\delta^{13}C$ values in some of the drusy mosaic calcite (Fig. 8) and blocky calcite cements (i.e., Group 2 in Fig. 9 and Table 1), compared to other cements, suggest that the bicarbonate required for the cement precipitation was derived from a 'marine' source. The $\delta^{13}C$ values fall well within the range of $\delta^{13}C$ values reported for the mid-Cretaceous marine carbonates (Arthur *et al*., 1988; Voigt, 2000). The calcite cement was derived mostly from marine carbonates with little or no modification in $\delta^{13}C$ values. The analyzed carbonate matrix and adjacent cements are isotopically different. Carbonate matrix commonly show values similar to those of normal sea water while the cement in some cases displays more positive $\delta^{13}C$ values (Table 1, 2.1 and 2.2). Such highly positive $\delta^{13}C$ values (i.e., +3.6‰ VPDB) observed in the cements could indicate precipitation from marine fluids characterized by positive carbon isotope excursion related to the Oceanic Anoxic Event (OAE) 2 for Cenomanian-Turonian (Arthur, *et al*., 1988; Scholle and Arthur, 1980).

Considering carbon as a major part of carbonate rocks and a minor component of basinal fluids, the $\delta^{13}C$ signature of carbonates is much less susceptible to alteration during water-rock interaction than $^{87}Sr/^{86}Sr$ or $\delta^{18}O$. Consequently, carbonate successions that undergo diagenetic stabilization with low water-rock ratios are unlikely to have $\delta^{13}C$ modified or homogenized. Magaritz (1983) found that $\delta^{13}C$ values will not appreciably decrease until the water-rock ratio is raised to 1000 or

more. This characteristic of $\delta^{13}C$ could explain the precipitation of most of the drusy mosaic calcite and Group 2 blocky calcite cement with $\delta^{13}C$ values similar to marine calcite while more depleted $\delta^{18}O$ values could indicate cement precipitation in mixed marine-meteoric realms.

A likely mechanism causing $\delta^{13}C$ depletion in Group 1 blocky and some drusy mosaic cements is meteoric diagenesis associated with sea level oscillations and episodic exposure of the Upper Sarvak platforms. The presence of paleoexposure surfaces and pedogenesis linked to the unconformity could have resulted in negative $\delta^{13}C$ values. The $\delta^{13}C$ values of carbonate cements precipitated under the influence of meteoric waters often are depleted due to influx of atmospheric-derived CO_2 with its distinctive low $\delta^{13}C$ values. This is further supported by the CL examination and Sr concentrations results (see Table 1). The zonation in drusy calcite cements also suggests their precipitation from fluids with varying concentrations of Mn and Fe (c.f. Veizer *et al*., 1999) and/or changes in the environmental conditions (see Machel *et al*., 1991).

The narrow range of $\delta^{13}C$ values observed from each blocky calcite cement generation (Group 1-3) indicates their precipitation from fluids with minor isotopic variations without organic carbon as a source for carbon.

The $\delta^{18}O$ of calcite is dependent on the temperature of precipitation and isotopic composition of the parent fluids. Assuming a temperature range of 15 to 36°C calculated for Mean Sea Surface Temperature (MSST) for Cenomanian-Turonian and during the deposition of the Sarvak Formation (Hajikazemi *et al*., 2010), the $\delta^{18}O$ of the calcite precipitated at these temperatures was determined using the equation of O'Neil *et al*., (1969).

$$1000 \ln \alpha = (\delta^{18}O_{Calcite} - \delta^{18}O_{water}) = 2.78 (10^6 T^{-2})-2.87 \qquad [1]$$

The marine calcite cements precipitated at the above temperatures, assuming seawater compositions for the mid-Cretaceous (no ice build-up) of -1.2 ‰ SMOW (White *et al*., 2001) would be characterized by $\delta^{18}O$ values range from -1.0 to -5.7‰ VPDB. It is important to note that the $\delta^{18}O$ values of the rudist shells fall within this range ($\delta^{18}O$ = -3‰ to -5.6‰). As a result, the majority of the cements which show $\delta^{18}O$

values between -2‰ and -5.5‰ VPDB (Table 1 and Fig.8), indicate their precipitation from fluids having an approximate seawater signature. $^{87}Sr/^{86}Sr$ ratios measured in these carbonate cements also vary little and fall well within the Cenomanian-Turonian portion of the secular seawater curve of Veizer *et al*. (1999) (see Table 1 for values).

More negative $\delta^{18}O$ values obtained for some cements could be explained either by precipitation from a fluid with lighter $\delta^{18}O$ values than coeval seawater or at higher temperature. $\delta^{18}O$-depleted meteoric water could conceivably infiltrated and diageneticaly modified Sarvak strata as a consequence of subaerial exposure due to sea-level fall combined with regional uplift. The $^{87}Sr/^{86}Sr$ ratios of some of the cements ($^{87}Sr/^{86}Sr$ >0.7084) are considerably more radiogenic than mid-Cretaceous sea water values determined previously (e.g., Derry *et al*., 1984; Veizer *et al*., 1999). These cements are closely associated with paleoexposure surfaces and have negative $\delta^{13}C$ values. Thus, the depleted $\delta^{18}O$ values of these calcite cements indicate a meteoric water influence.

During the mid-Cretaceous, the area was located in a warm equatorial region. The $\delta^{18}O$ of meteoric water existed at this time could not have been less than -6‰ (White *et al*., 2001), while the global average temperature ranged from 12 to 20.8 °C (Frakes *et al*, 1992; Donnadieu *et al*., 2006). Calcite cements precipitated in equilibrium with meteoric waters could have $\delta^{18}O$ values around -6.0 ± 1‰. The $\delta^{18}O$ of pedogenic carbonates ranging from -5.2 to -3.7‰, which certainly indicates meteoric water influence also agree with such an interpretation. Additionally, the $^{87}Sr/^{86}Sr$ ratios of these pedogenic carbonates ($^{87}Sr/^{86}Sr$ >0.70812 and 0.70817) are more radiogenic than the mid-Cretaceous marine values. The pore water at this time was probably an isotopically evolved mixture of marine and meteoric-derived waters; with a major contribution of meteoric- derived water close to the unconformity surface (s) and greater component of marine- derived pore water down section.

Deposition of the Laffan shales and Ilam carbonates (in the Persian Gulf area) or the Gurpi Formation (at the type section), on top of the Sarvak Formation, following extensive uplift and subaerial exposure, indicates that the Sarvak Formation was flooded by marine water and additionally the platform may have been subjected to

burial diagenesis. Precipitation of calcite cements with $\delta^{18}O$ as negative as -12‰, could be explained either by an increase in temperature, or by a progressive change in the isotopic composition of the pore waters, or by a combination of both. Meteoric diagenesis of marine carbonates typically results in a shift towards more negative values of both $\delta^{18}O$ and $\delta^{13}C$ (Anderson and Arthur, 1983), whereas burial diagenesis produces larger shifts in $\delta^{18}O$ values than meteoric diagenesis, with no significant changes in $\delta^{13}C$ values (e.g. Choquette and James, 1987). Based on calculations utilising $\delta^{18}O$ values of cements, the maximum possible temperature during precipitation of these depleted cements is between 50°C and 85°C. This is also in accordance with the presence of two-phase fluid inclusions in some of the blocky cements, indicating their formation under higher ambient temperatures compared to earlier generations of cements. Thus, we assume that the minimum temperatures for the calcite precipitation would be at least 50°C, corresponding to about 1 km depth of burial at the time of precipitation of these cements. Figure 12 illustrates the evolution of calcite cement from marine to meteoric and burial diagenetic environment.

Dolomite

Possible carbon sources for dolomite include dissolved bicarbonate from normal marine water or bicarbonate production related to the modification of organic matter. Considering the $\delta^{13}C$ values of the dolomites (i.e., 2.0-5.0 ‰VPDB) a marine source can be suggested for their carbon.

The $\delta^{18}O$ values of dolomites are lower than values for mid-Cretaceous marine carbonates (Table 1). Such low values are not expected for dolomite compared to calcite theoretically co-precipitated from the same parent fluids (Land, 1985). In such a case dolomite should be enriched in^{18}O and have $\delta^{18}O$ values about 4‰ more positive relative to calcite (Hoefs, 1987). Thus, based on the $\delta^{18}O$ values obtained from calcite and dolomites, it can be concluded that they have been precipitated in different stages from different sources.

The range of $\delta^{18}O$ values for these dolomites probably reflects varying compositions or temperatures of the waters involved. Using the paleotemperature equation for dolomite (Land, 1985) [2], we can employ measured $\delta^{18}O$ values (ranging from -6.7‰ to -2.7‰ VPDB) to estimate the water's $\delta^{18}O$.

$T^{o}C = 16.4 - 4.3 ([\delta^{18}O_{dol} - 3.8] - \delta^{18}O_{Water} + 0.14([\delta^{18}O_{dol} - 3.8] - \delta^{18}O_{Water})^2$ [2]

Where *T* is temperature (in ºC), $\delta^{18}O_{dol}$ is the oxygen isotope value in studied samples (in PDB), $\delta^{18}O_{Water}$is the oxygen isotope value of marine water (in SMOW). The calculations show temperature between 35- 80^{o}C for the parent fluids of the dolomites.

It is reasonable to assume that the dolomite formed from marine to mixed marine-meteoric waters under relatively warm temperatures. Due to crystal shape and size of the dolomites and also above mentioned temperatures, it is unlikely that the dolomite precipitated directly from marine or meteoric waters. We conclude that dolomite was formed from mixed marine-meteoric pore water with temperatures ranging from 35 to 80°C. Based on the obtained geochemistry data and occurrence of the examined dolomites after stylolite formation, it could be interpreted that they formed in a burial diagenetic environment. Assuming a 15°C mean annual surface temperature and a 30°C /km geothermal gradient, a minimum of 2 km of sediments would need to have been deposited to satisfy the maximum temperatures (i.e., 80°C) proposed here, if burial heating alone were the mechanism responsible. This burial constraint suggesting 2 km or more of sediments are inconsistent with the known stratigraphy for the region. Since the sufficient depth of burial were not reached until Miocene time in southern Iran (Kamalee and Rezaei, 2003; Sharp *et al*., 2010) an upward migration of warm hydrothermal fluids to shallower depths can also be envisaged. Therefore, the proposed temperatures are not representative of heating because of burial alone, but instead are caused by increased local or regional geothermal gradient related to fluid flow and moving hot brines from greater depths upward into the Sarvak Formation.

CONCLUSIONS

Petrographic and geochemical study of shallow-water carbonates of the mid-Cretaceous Sarvak Formation from southern Iran record a diagenetic history which can be summarized as follows:

(1) Deposition of shallow-marine carbonates of the Upper Sarvak Formation during the Cenomanian- Turonian and early marine cementation;

(2) Tectonic uplift and salt diaprism in late Cenomanian causing subaerial exposure of the Sarvak Formation at Cenomanian-Turonian boundary, that allowed the influx of meteoric water into the carbonates causing vast dissolution and reservoir properties enhancement and also precipitation of some calcite cements;

(3) Marine transgression and sea-level rise during the early Turonain and precipitation of later marine cements in pores and some fractures;

(4) Sea-level fall during mid-Turonian resulting in the regional Turonian unconformity, which caused paleoexposure and deep erosion and removal of the carbonates and their dissolution and creation, enhancement and development of effective porosity and favourable reservoir characteristics.

(5) Burial of the platform with circulating sea-water providing a site for dolomitization and also precipitation of the last generation of blocky calcite cement in some pore spaces.

(6) Early diagenetic cements were formed at low to moderate temperatures (<50°C) during sediment compaction; late diagenetic cements (i.e., blocky calcite), dolomite and coarse crystalline pyrite precipitated at higher temperatures (~50°–80°C) during deeper burial.

(7) Dissolution due to invading of meteoric waters is the main reservoir property enhancement; and dolomitization can be considered as the other factor but in lesser extent.

ACKNOWLEDGMENTS

We would like to thank IOOC, NIOC and NISOC for their kind assistance and help with field work and for access to the core laboratory. Constructive comments by the Marine and Petroleum Geology reviewers are greatly appreciated. Funding for the project was provided by StatoilHydro. Additional funding was provided by Natural Science and Engineering Research Council of Canada (NSERC) to I. S. Al-Aasm and M. Coniglio.

REFERENCES

AL-AASM, I.S. and VEIZER, J., 1986b.Diagenetic stabilization of aragonite and low-Mg calcite, II. Stable isotopes in rudists. Journal of Sedimentary Petrology, 56, 763-770.

AL-AASM, I. S., TYLOR, B. E. and SOUTH, B., 1990. Stable isotope analysis of multiple carbonate samples using selective acid extraction. Chemical Geology, 80, 119-125.

ANDERSON, T. F. and ARTHUR, A. 1983.Stable isotopes of oxygen and carbon and their application to sedimentologic and paleoenvironmental problems. In Stable Isotopes in Sedimentary Geology. SEPM Short Course 10. 111-151.

ARTHUR, M.A., DEAN, W.E. and PRATT, L.M., 1988. Geochemical and climatic effects of increased marine organic carbon burial at the Cenomanian-Turonian boundary. Nature, 335, 714–717.

ASGHARI, M., ADABI., M. H. ADABI 2014. Diagenesis and Geochemistry of the Sarvak Formation in Ahvaz oil field-Iran. Geochemistry Journal, 1, Issue 1.

BARRERA, E., and G. KELLER (1990), Stable Isotope Evidence for Gradual Environmental Changes and Species Survivorship across the Cretaceous/Tertiary Boundary, Paleoceanography, 5(6), 867–890.

BEIRANVAND, B. AHMADI, A. and SHARAFODIN, M. 2007. Mapping and classifying flow units in the upper part of the Middle Cretaceous Sarvak formation (western Dezful Embayment, SW Iran) based on a determination of the reservoir types. Journal of Petroleum Geology. 30, 4, 357-373.

CHOQUETTE, P. W. and JAMES, N. P. 1987.Limestones 3, The deep burial environment. Geoscience Canada 14, 3-35.

DERRY, L.A., BRASIER, M.D., CORFIELD, R.M., ROZANOV, A. YU. and ZHURAVLEV, A. U.,1984. Sr and C isotopes in Lower Cambrian carbonates from the Siberian craton: A paleoenvironmental record during the'Cambrian explosion' Earth and Planetary Science Letters. 128, 671-681

DONNADIEU, Y, PIERREHUMBERT, R., JACOB, R., and FLUTEAU, F., 2006. Modelling the primary control of paleogeography on Cretaceous climate. Earth and Planetary Science Letters, 248, 426-437.

ESRAFILI-DIZAJI, B., RAHIMPOUR-BONAB, H., MEHRABI, H. 2015. Characterization of rudist-dominated units as potential reservoirs in the middle Cretaceous Sarvak Formation, SW Iran. Facies, 61(3), 1-25.

FARZADI, P. and HESTHMER, J. 2007. Diagnosis of the Upper Cretaceous palaeokarst and turbidite systems from the Iranian Persian Gulf using volume-based multiple seismic attribute analysis and pattern recognition. Petroleum Geoscience, 13, 227-240

FRAKES, L.A., FRANCIS, J.E. and SYKTUS, J.I., 1992. Climate modes of the Phanerozoic, Cambridge University Press. 274p.

GHAZBAN, F. 2007. Petroleum geology of the Persian Gulf. Joint publication, Tehran University Press and National Iranian Oil Company. 706p.

HAJIKAZEMI, E., AL-AASM, I.S., and CONIGLIO, M, 2012. Chemostratigraphy of Cenomanian- Turonian Carbonates of the Sarvak Formation, Southern Iran, Journal of Petroleum Geology. 35(2), 187-206

HAJIKAZEMI, E., AL-AASM, I. S., and CONIGLIO, M, 2010. Subaerial Exposure and Meteoric Diagenesis of the Cenomanian-Turonian Upper Sarvak Formation, southwestern Iran. In: Leturmy, P. and Robin, C. (Eds), Tectonic and Stratigraphic Evolution of Zagros and Makran during the Mesozoic-Cenozoic. Geol. Soc.Lond. Spec. Publ. 330.

HAJIKAZEMI, E., GHAZBAN, F.YOUSEFPOOR, M.R., 2002. Depositional and Diagenetic History of the Cretaceous Sedimentary Sequence in Sirri Oil Field in the Persian Gulf, Iran,The 3rd Middle East and North Africa Oil and Gas Conference (MENA), Imperial College, London.

HARRIS, P. M. and FROST, S. H. 1984. Middle Cretaceous Carbonate Reservoirs Fahud Field and Northwestern Oman. AAPG Bull. 68, 649-658

HOEFS, J., Stable isotope geochemistry, 1987, Springer, 285p.

Hollis, C., 2011. Diagenetic controls on reservoir properties of carbonate successions within the Albian-Turonian of the Arabian Plate. Petroleum Geoscience, 17(3), 223-241

IMMENHAUSER, A., NAGLER, T.F., STEUBER, T. and HIPPLER, D. 2005. A critical assessment of mollusk $^{18}O/^{16}O$, Mg/Ca, and $^{44}Ca/^{40}Ca$ ratios as proxies for Cretaceous seawater temperature seasonality. Palaeogeography, Palaeoclimatology, Palaeoecology, 215, 221– 237.

JAMES, N.P. and CHOQUETTE, P.W. 1990: Limestone diagenesis, the meteoric environment. In: Sediment diagenesis. (I. McIlreath and D. Morrow, Eds),. Geological Association Canada, Reprint Series 4, 36–74.

JENKYNS, H. C., GALE, A. S. and CORFIELD, R. M. 1994. Carbon and oxygen isotope stratigraphy of the English Chalk and Italian Scaglia and its palaeoclimatic significance. Geological Magazine 131, 1–34.

KAMALEE, M. R., and REZAEI, M.R 2003.Burial history reconstruction and thermal modelling at kuh-e Mond, SW Iran.Journal of Petroleum Geology.Volume 26, 4.P 451–464

KOOP, W. and STONELEY, R., 1982. Subsidence history of the Middle East Zagros Basin, Permian to Recent. Phil. Trans. Roy. Soc. Lond., 305, 149–168.

LAND, L.S., 1985. The origin of massive dolomite. Journal of Geological Education, 33, 112–125.

MACHEL, H.G., MASON, R.A., MARIANO, A.N. and MUCCI, A., 1991. Causes and emission of luminescence in calcite and dolomite. In: C.E. Barker and O.C. Kopp (Editors), Luminescence Microscopy and Spectroscopy: Qualitative and Quantitative Applications. SEPM Short Course, 25, 9-25.

MAGARITZ, M.,1983. Carbon and oxygen isotope composition of recent and ancient coated grains, in Peryt, T.M., ed., Coated grains: Berlin, Springer-Verlag, 27-37.

MARSHALL, J. D., 1992, Climatic and oceanographic signals from the carbonate rock record and their preservation: Geological Magazine, 129, 143–160.

MEHRABI, H., RAHIMPOUR-BONAB, H., 2014. Paleoclimate and tectoniccontrols on the depositional and diagenetic history of theCenomanian-early Turonian carbonate reservoirs, DezfulEmbayment, SW Iran. Facies, 60,147–167

MEHRABI, H., RAHIMPOUR-BONAB, H., HAJIKAZEMI, E., 2015, Controls on depositional facies in Upper Cretaceous carbonate reservoirs in the Zagros area and the Persian Gulf, Iran.Facies, 61(4), 1-24.

MORAD, S., AL-AASM, I.S., RAMSEYER, K., MARFIL, R. and ALDAHAN, A.A., 1990.Diagenesis of carbonate cements in Permo-Triassic sandstones from the IberianRange, Spain: evidence from chemical composition and stable isotopes. Sedimentary Geology. 67, 281- 295.

MOTIEI, H, 1993. Geology of Iran. The stratigraphy of Zagros. Geological survey of Iran (in Farsi).

O'NEIL J. R., CLAYTON R. N. and MAYEDA T. K. 1969. Oxygen isotope fractionation in divalent metal carbonates. Journ. Chem. Phys. 51, 5547–5558.

SAVARD, M.M., VEIZER, J. and HINTON, R., 1995. Cathodoluminescence at low Fe and Mn concentrations: A SIMS study of zones in natural calcites: Journal of Sedimentary Research, ser. A, 65, 208–213.

PIRYAEI, A., REIJMER, J. J. G., VAN BUCHEM, F. S. P., YAZDIMOGHADAM, M., SADOUNI, J. and DANELIAN, T. ,2010.The influence of Late Cretaceous tectonic processes on sedimentation patterns along the northeastern Arabian plate margin (Fars Province, SW Iran). In: Leturmy, P. andRobin, C. (Eds), Tectonic and Stratigraphic Evolution of Zagros and Makran during the Mesozoic-Cenozoic. Geol. Soc. Lond. Spec. Publ. 330.

PIRYAEI, A., REIJMER, J.G., BORGOMANO J, VAN BUCHEM FSP. 2011. Late Cretaceous tectonic and sedimentary evolution of the Bandar Abbass area, Fars region, southern Iran. J Pet Geol 34(2), 157–180

SCHOLLE, P. A. and ARTHUR, M. A. 1980: Carbon isotope fluctuations in cretaceous pelagic limestones: Potential stratigraphic and petroleum exploration tool. AAPG Bull., 64, 67-87.

SETUDEHNIA, A. 1978. The Mesozoic succession in S.W. Iran and adjacent areas. Journal of Petroleum Geology, 1, 3-42.

SHARP, I., GILLESPIE, P., MORSALNEZHAD, D., TABERNER,C., KARPUZ, R., VERGES, J., HORBURY A., PICKARD, N.,GARLAND, J. and HUNT, D., 2010. Stratigraphic architecture and fracture-controlled dolomitization of the Cretaceous Khami and Bangestan groups: an outcropcase study, Zagros Mountains, Iran. In: van Buchem, F. S. P., Gerdes, K. D. and Esteban, M. (Eds.), Mesozoic and Cenozoic Carbonate Systems of the Mediterranean and the Middle East: Stratigraphic and Diagenetic Reference Models. Geol. Soc. Lond. Spec. Publ., 329, 343-396.

STEUBER, T., 1996. Stable isotope sclerochronology of rudist bivalves: growth rates and Late Cretaceous seasonality. Geology, 24, 315–318.

TAGHAVI, A.A., MORK, A, and EMADI, M.A., 2006. Sequence stratigraphically controlled diagenesis governs reservoir quality in the carbonate Dehluran Field, southwest Iran, Petroleum Geoscience, 12(2), 115-126.

Van Buchem, F., Gaumet,F, Vedrenne, V., Vincent, B. 2006. Middle East Cretaceous sequence stratigraphy study. NIOC-IFP unpublished report.

VEIZER, J., 1983b, Chemical diagenesis of carbonates: Theory and application of trace element technique, in Stable isotopes in sedimentary geology: Society of Economic Paleontologists and Mineralogists Short Course 10, 3.1– 3.100.

VEIZER, J., ALA, D., AZMY, K, BRUCKSCHEN, P., BUHL, D., BRUHN, F., CARDEN, G.A.F., DIENER, A., EBNETH, S., GODDERIS, Y., JASPER, T., KORTE, C., PAWELLEK, F., PODLAHA, O.G. and STRAUSS, H. 1999. $^{87}Sr/^{86}Sr$, $\delta^{13}C$ and $\delta^{18}O$ evolution of Phanerozoic sea water. Chemical Geology, 161, 59–88.

VIDETICH, P.E.,MCLIMANS, R.K., WATSON, H.K. & NAGY, R.M. 1988. Depositional, diagenetic , thermal and maturation histories of Cretaceous Mishrif Formation, Fateh Field, Dubai. American Association of Petroleum Geologists Bulletin, **72**, 1143-1159.

VINCENT, B., VAN BUCHEM, F S.P., BULOT L. G., JALALI, M., SWENNEN, R., HOSSEINI, A.S. AND BAGHBANI, D., 2015.Depositional sequences, diagenesis and structural control of the Albian to Turonian carbonate platform systems in coastal Fars (SW Iran), Marine and Petroleum Geology 63 (2015), 46-67.

VOIGT, S., 2000. Cenomanian–Turonian composite $\delta^{13}C$ curve for Western and Central Europe: the role of organic and inorganic carbon fluxes. Palaeogeography, Palaeoclimatology, Palaeoecology. 160, 91–104.

WHITE, T., GONZALES, L., LUDVIGSON, G. and POULSON, C., 2001. Middle Cretaceous greenhouse hydrologic cycle of North America. Journal of Geology, 29, 363-366.

Sample No.	^{43}Ca	^{55}Mn	^{86}Sr	$^{87}Sr/^{86}Sr$	$\delta^{13}C$	$\delta^{18}O$
8700-C	363739	14	112		-1.6	-5.9
9211-C					2.2	-2.2
9447-C					2.1	-6.4
9441.8-C	270744	15	202	0.70745	1.8	-5.9
8955-C	281240	22	34		-0.3	-4.8
8446-C	297866	17	59		-5.8	-6.5
8447-C	283751	23	112		-3.5	-5.6
8447-C					-3.8	-5.8
8700-C	274763	10	102	0.70717	-2.4	-5.4
9428-C	252884	8	169		2.0	-5.0
9438-C	311404		70		3.1	-0.6
8943-C					0.4	-3.9
8961-C					2.2	-5.0
8185-C	279219	17	86	0.70747	0.8	-5.1
2517-C					2.1	-3.8
7354-C					2.9	-2.3
7423-C					2.9	-6.5
7464-C					2.8	-5.7
2520-C					1.7	-4.8
167-C	254058	18	277		0.1	-6.2
165-C	311181	14	166	0.70731	0.0	-4.4
161-C	321049	18	169	0.70745	-1.1	-1.9
160-C	278844	8	281		-1.0	-1.6
159-C	287371	5	266		1.5	-1.8
158-C					3.4	-3.7
157-C					3.4	-3.7
155-C	325269	9	213	0.70729	0.6	-2.3
153-C	281752	18	146	0.70846	0.7	-2.2
147-C				0.70746	1.8	-3.1
143-C	223250	4	51	0.70771	2.8	-3.2
140-C	600350	21	225	0.70766	3.0	-2.8
139-C					2.4	-1.8
134-C					2.4	-3.5
132-C	312811	22	214	0.70762	2.9	-3.3
129-C	290026	6	195	0.70732	3.5	-5.2
128-C	292198	3	55		2.9	-4.0
120-C	278000	5	222	0.70731	2.5	-3.0

Table 1 (Continued)

114-C	276639	5	137		2.2	-1.2
111-C	310488	6	213	0.70775	-0.6	-8.9
109-C	203820	4	30	0.71015	3.3	-1.4
108-C	317418	4	147	0.71016	1.4	-4.3
102-C	287798	3	306	0.70728	2.0	-2.4
99-C	347276	4	212	0.70746	2.3	-1.8
97-C				0.70718	2.2	-2.5
95-C	306083	3	136	0.70714	1.4	-2.1
94-C	88971	2	118		3.1	-1.6
88-C				0.70772	1.5	-4.7
89-C				0.70756	0.8	-5.3
71-C					1.9	-4.0
57-C					3.2	-3.9
RU-B	281592	33	101		2.1	-6.0
BH-104-B	281028	44	56	0.70731	1.8	-5.3
BH-104-B					0.8	-5.6
BH-104-B					1.6	-5.9
BH104-CB					2.0	-5.7
BH105-CB					1.5	-6.0
BH-4-B	252204	29	105	0.70752	1.9	-6.2
BH106-B					0.9	-9.3
BH-2-B					2.5	-4.9
BH-12-B					2.1	-6.4
BH101-B					1.3	-4.1
BH-0-B					2.2	-6.7
BH-4-B	281839	33	101		2.1	-6.6
106-B					1.8	-4.6
140-B					2.2	-5.9
BH106-B					1.4	-12.3
9211.5-B					1.9	-1.8
8955-B	240743	21	168		-1.4	-5.9
2514-B	296480	12	100	0.70743	3.0	-3.7
10107-B	233474	11	85	0.70747	2.4	-3.0
9214-B					0.0	-6.7
8700-B	293239	10	117	0.70745	-2.4	-5.4
7351-B					3.5	-3.5
8943-B	292706	30	89		0.2	-3.4

Table 1 (Continued)

8688-B	288118	18	72		0.3	-3.4
110-B	177294	3	52		2.2	-4.7
163-B	313373	6	484	0.70745	0.5	-8.0
9442-B	393586	11	260	0.70745	1.7	-6.4
8173-B	281557	11	680	0.70717	2.1	-4.8
8951-B	298215	34	129		2.2	-5.0
28-B	245837	30	138		2.1	-6.2
8952-B					1.3	-5.4
165-B					0.5	-8.0
7465-B					3.6	-3.9
BH-2-B					2.5	-5.7
7348-dol					3.4	-3.5
7468-dol					2.0	-6.7
7465-dol					3.2	-3.4
7253-dol					2.2	-5.7
9809-dol					4.4	-4.2
9791.2-dol					4.8	-3.7
9799-dol					4.6	-3.8
9815-dol					5.0	-4.2
9441.8-dol					3.4	-3.1
9425-dol					3.0	-2.7

Table.1 Stable isotope values and elemental concentration of drusy mosaic (C), blocky calcite (B) cement and dolomite (dol) of the Sarvak Formation in the study area. C: Drusy mosaic calcite cement; B: Blocky calcite cement; dol: Dolomite

Table 2.1

Sample No.	$\delta^{13}C$ (PDB)	$\delta^{18}O$ (PDB)	$^{87}Sr/^{86}Sr$	Sr (ppm)	Mn (ppm)
167-M	-0.3	-4.5	0.70878	154	13
166-M	-0.3	-3.4	0.70731	114	15
165-M	0.2	-2.1	0.70756	234	12
164-M	1.5	-2.3	0.70753		
163-M	0.6	-3.4	0.70733	422	17
162-M	1.7	-3.9			
161-M	2.3	-2.3		196	5
159-M	1.7	-2.7		298	6
157-M	1.5	-3.0			
155-M	0.2	-2.8	0.70751	303	9
151-M	-0.1	-3.1	0.70748	315	12
150-M	2.0	-1.1		306	5
143-M	2.1	-0.9	0.70755	235	4
140-M	2.4	-1.7		356	10
139-M	2.4	-1.6		280	20
134-M	2.0	-3.7	0.70766	288	9
132-M	2.6	-1.0			
129-M	2.4	-3.6	0.70755	252	7
128-M	2.6	-3.9		244	8
120-M	2.4	-1.2		117	2
114-M	2.5	-3.4	0.70754	254	3
111-M	2.3	-3.6	0.70741	213	5
110-M	2.3	-3.1			
109-M	2.2	-2.5			
108-M	1.2	-5.9			
106-M	2.2	-2.9			
105-M	2.2	-2.0			
102-M	2.6	-1.7	0.70728	236	4
97-M	1.9	-4.0	0.70755	377	4
95-M	2.3	-3.7		293	5
94-M	1.9	-3.6		327	11
88-M	0.5	-5.6		215	8
87-M	0.5	-4.5		159	3
83-M	1.8	-3.7	0.70761	276	3
80-M	3.3	-5.2		363	4
74-M	0.8	-5.4		260	3
71-M	1.5	-4.2	0.70745	242	2
69-M	1.8	-4.4		340	6
62-M	1.8	-4.4	0.70784		
58-M	2.2	-4.0			
54-M	0.3	-6.5		552	4
51-M	1.7	-4.6			
49-M	1.0	-5.8	0.70745		
36-M	-0.7	-9.4	0.70740	1298	16

Table 2.1(Continued)

Sample No.	$\delta^{13}C$ (PDB)	$\delta^{18}O$ (PDB)	$^{87}Sr/^{86}Sr$	Sr (ppm)	Mn (ppm)
32-M	1.4	-4.1			
27-M	1.2	-4.3			
21-M	0.9	-8.6	0.70743	1336	16
16-M	1.7	-4.4	0.70745	800	21
EH-2-M	2.6	-4.4			
EH-3-M	2.4	-5.2			
EH-4-M	2.1	-5.6			
EH-5-M	1.6	-4.3			
EH-6-M	1.5	-4.2			
EH-7-M	2.2	-5.3			
EH-9-M	2.5	-4.5		169	23
EH-10-M	-3.0	-4.2			
EH-11-M	0.8	-6.3			
EH-12-M	1.5	-4.2			
EH-13-M	2.5	-4.7			
SE-21-M	-5.8	-4.6		127	170
SE-22-M	-1.6	-4.5			
SE-23-M	0.6	-5.6			
SE-28-M	2.7	-5.1			
SE-29-M	2.4	-6.2			
BH-0-M	2.6	-4.4		144	18
BH-2-M	2.4	-4.8			
BH-3-M	1.6	-5.3			
BH-6-M	1.5	-4.2		164	35
BH-12-M	2.5	-4.7			
BH-107-M	0.8	-6.3			
BH-106-M	2.9	-5.4			
BH-104-M	2.3	-5.2	0.70749		
SK1-M	-3.4	-6.2			
SK2-M	-3.0	-5.8			
SK3-M	3.1	-5.2			
BH-5-P	-3.0	-4.2			
SS-1-P	-5.4	-3.7	0.70813		
SS-2-P	-1.6	-4.1			
SS-3-P	-7.3	-4.7			
SS-5-P	-9.1	-5.2			
SS-6-P			0.70818		

Table 2.1 Carbon, Oxygen and Sr isotopic values and elemental concentrations of calcite matrix and palaeosol from surface sections. M: Matrix, P: Palaeosol

Table 2.2

Sample No.	$\delta^{13}C$ (PDB)	$\delta^{18}O$(PDB)	$^{87}Sr/^{86}Sr$	Sr (ppm)	Mn (ppm)
Bibi Hakimeh					
1-M	2.0	-4.0	0.707454	463	13
2-M	1.9	-3.8	0.707422		
3-M	2.2	-4.2			
4-M	2.1	-4.0	0.70777		
5-M	2.5	-4.2			
6-M	2.6	-4.6	0.70748		
7-M	2.3	-5.7	0.70742		
8-M	2.6	-4.7	0.70737		
9-M	3.6	-4.6		517	7
10-M	3.3	-4.1			
11-M	1.8	-6.9			
12-M	2.8	-5.0			
13-M	1.5	-6.5			
14-M	1.5	-6.5			
15-M	3.5	-4.4			
16-M	3.4	-3.8	0.70728	479	21
Sirri-D					
1-M	1.8	-5.1	0.70753	169	35
2-M	1.7	-5.1	0.70747		
3-M	1.8	-5.3	0.70788		
4-M	2.0	-5.1			
5-M	2.1	-5.3	0.70744		
6-M	2.1	-5.0	0.70754		
7-M	1.7	-5.2			
8-M	2.6	-5.0			
Rag-e Sefid A					
1-M	-4.8	-6.1	0.70732	197	28
2-M	-6.4	-6.1			
3-M	-0.6	-5.8	0.70833		
4-M	1.9	-2.7			
5-M	1.7	-3.2			
6-M	-1.0	-6.7		264	14
7-M	1.5	-3.1			
8-M	-0.6	-5.2			
9-M	-0.4	-3.8	0.70740	314	38
10-M	1.9	-3.7			
11-M	1.3	-3.7		254	21
12-M	1.2	-4.2	0.70729		
13-M	1.0	-3.8			
14-M	1.4	-3.6			
15-M	3.9	-3.8		327	2
16-M	1.4	-4.0		309	12
17-M	2.3	-3.8		263	8
18-M	1.9	-3.7			

Table 2.2 (Continued)

Sample No.	$\delta^{13}C$ (PDB)	$\delta^{18}O$ (PDB)	$^{87}Sr/^{86}Sr$	Sr (ppm)	Mn (ppm)
19-M	1.9	-5.1			
20-M	2.1	-3.8		218	20
21-M	2.2	-3.3			
22-M	2.2	-4.5	0.70743		
23-M	4.1	-3.8		338	3
24-M	4.0	-4.0	0.70712	407	3
25-M	3.7	-4.0			
26-M	3.8	-3.7		229	3
27-M	2.5	-3.9	0.70723		
Rag-e Sefid B					
1-M	2.7	-3.8			
2-M	2.7	-4.4	0.70746		
3-M	2.8	-4.1			
4-M	3.0	-3.2	0.70754		
5-M	2.4	-5.3			
6-M	2.6	-4.2			
7-M	2.3	-3.7	0.70729		
8-M	2.4	-2.8			
9-M	2.2	-4.0			
10-M	2.9	-3.5			
11-M	2.6	-3.9			
Rudist Shell					
91-Sh	2.0	-3.7		340	10
92-Sh	1.9	-3.3	0.70740	349	2
98-Sh	1.8	-3.0	0.70736	319	4
8154-Sh	1.3	-5.2	0.70748	197	14
8217-Sh	2.4	-4.9	0.70717		
8173-Sh	1.7	-5.2	0.70714		
2514-Sh	2.7	-5.0	0.70750		
7404-Sh	2.6	-4.6			
8952.8 Sh	2.1	-3.6			
9438-Sh	1.8	-5.6			
9791-Sh	1.6	-5.3			
10102-Sh	2.4	-5.0			
10120-Sh	2.5	-5.2			
RV-1-Sh	2.0	-4.4	0.70750		
RV-2-Sh	2.1	-4.3			
RV-3-Sh	2.0	-4.5			
R-H-1-Sh	1.9	-4.9		354	37
R-H-2-Sh	1.8	-5.3			
R-H-3-Sh	1.5	-5.3			
BH-104-Sh			0.70749		

Table 2.2 Carbon, Oxygen and Sr isotopic values and elemental concentrations of rudist shells and calcite matrix from core samples

Sh: rudist shell M: Calcite Matrix

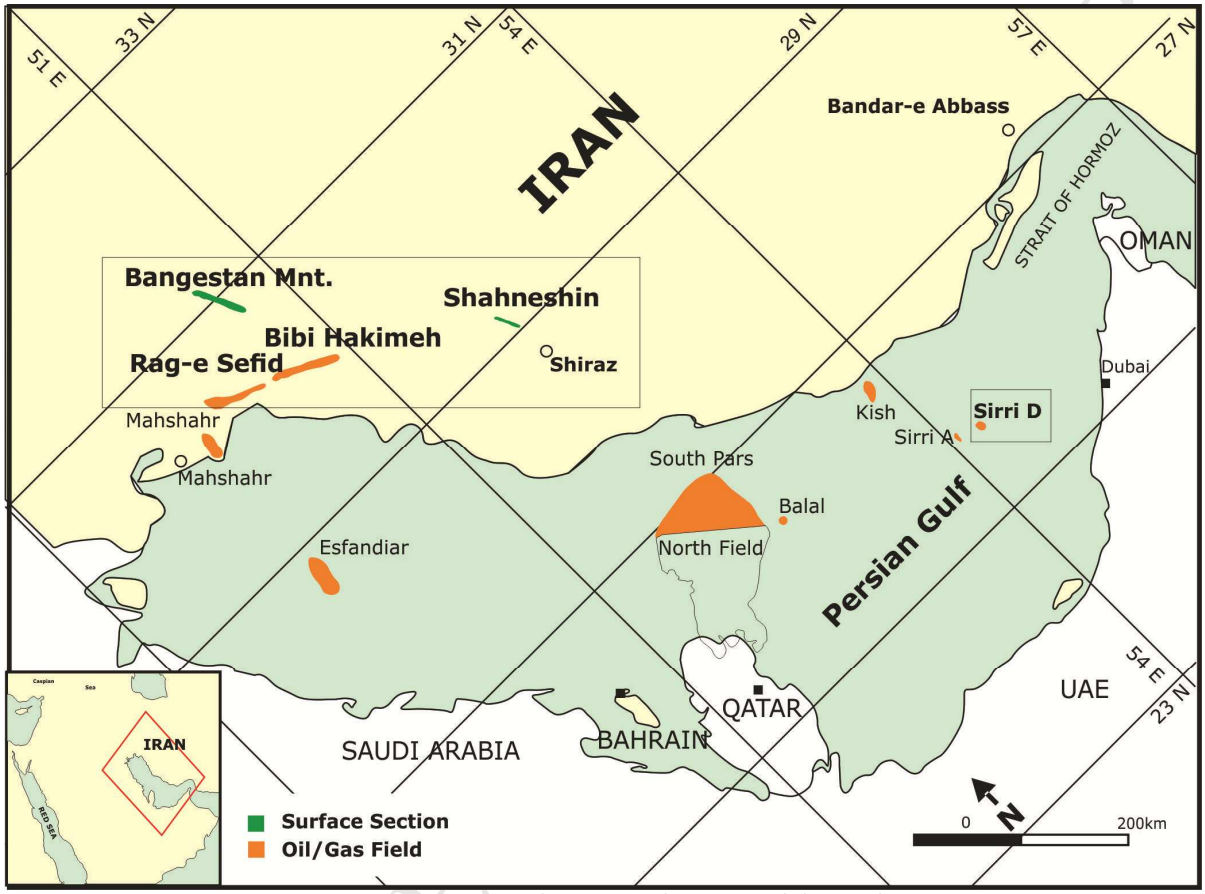

Fig. 1 Location map of the study area

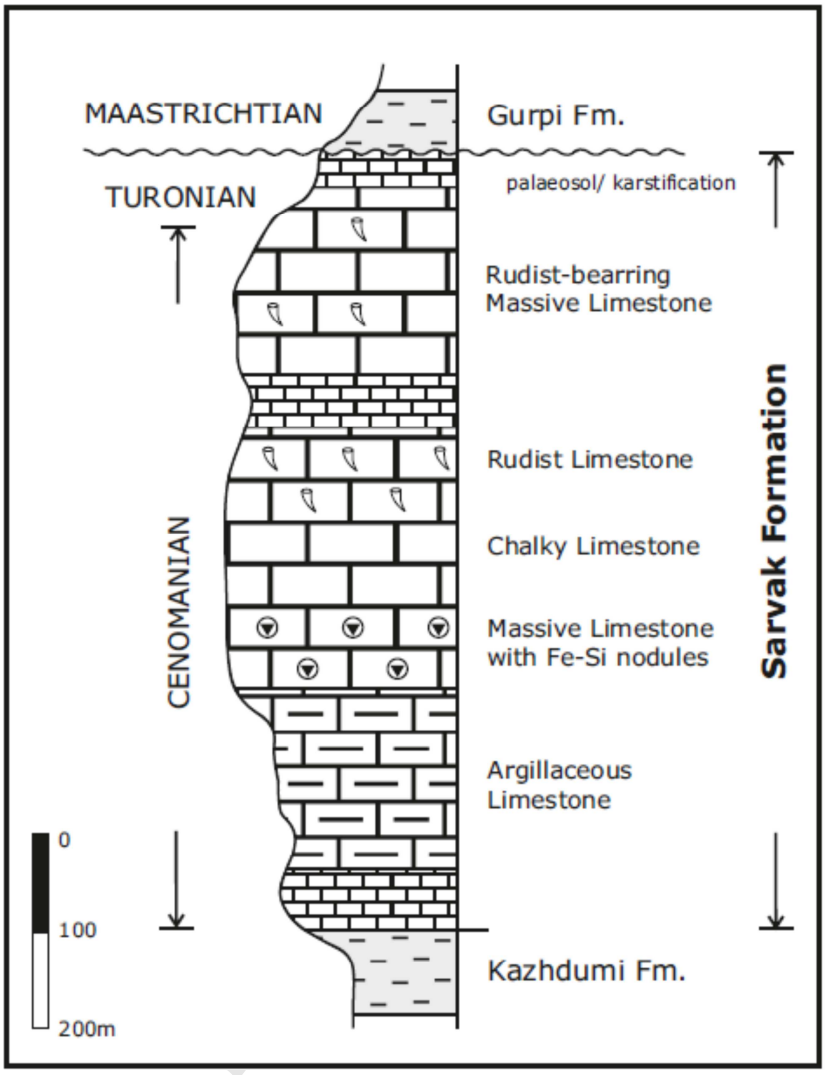

Figure 2 Stratigraphy column of the Sarvak Formation at the type section, Bangestan Mountain

(modified from Motiei, 1993)

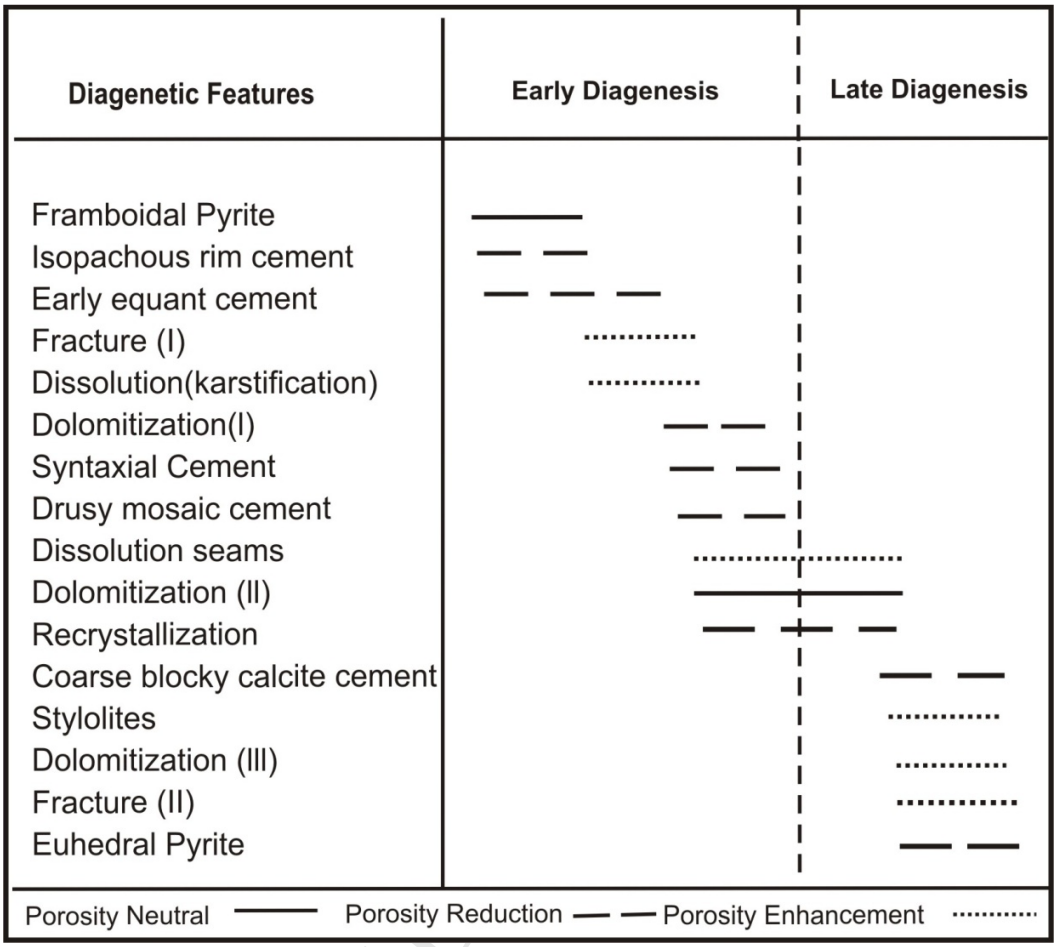

Fig.3 Paragenetic sequence of the most important diagenetic features of the Sarvak Formation

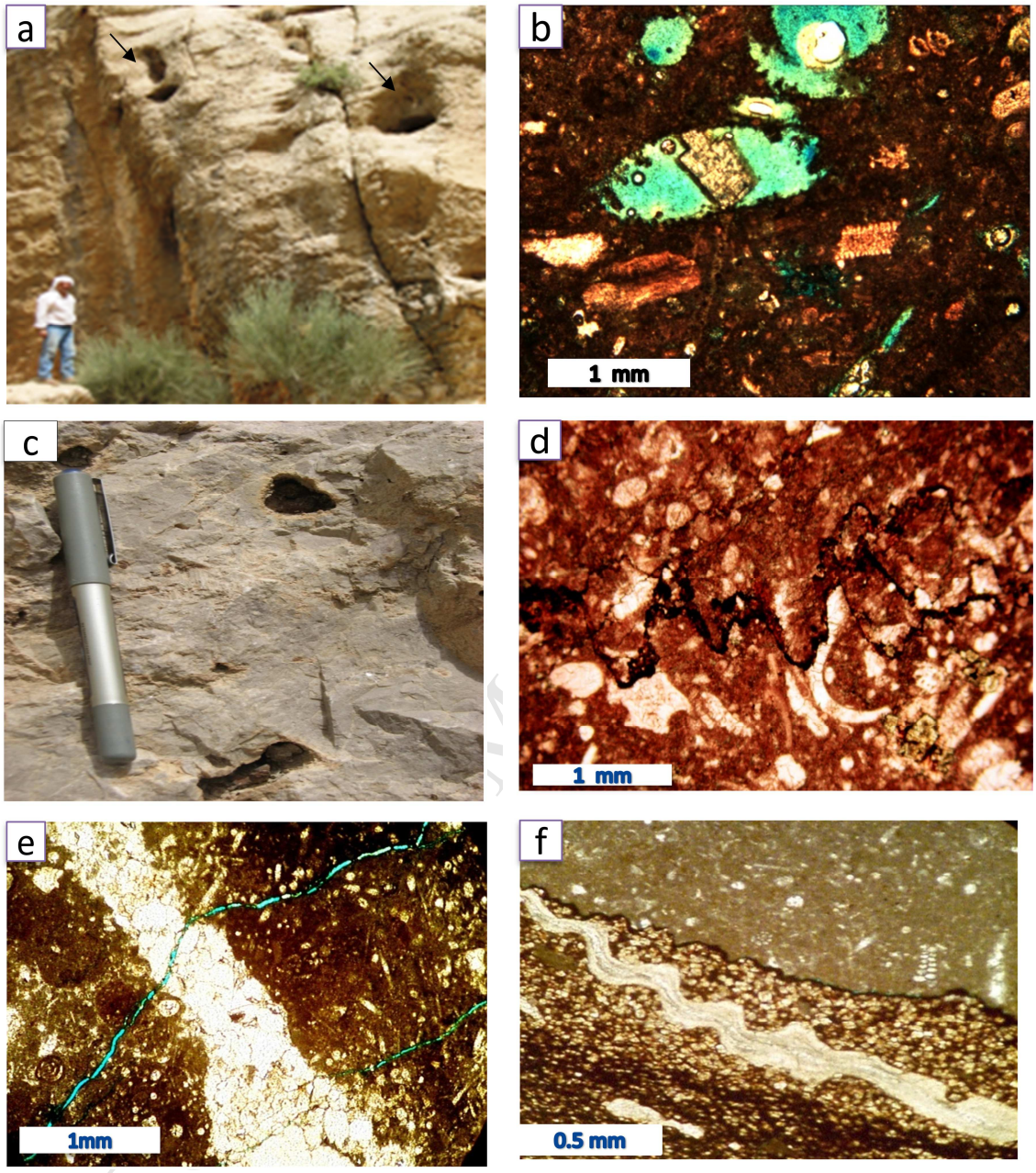

Figure 5. a) Cavernous porosity below the unconformity surface in Shahneshin Mountain, b) Mouldic porosity partially filled with calcite cement, c) Vuggy porosity below the unconformity surface in Shahneshin Mountain d) Foraminifera packstone with stylolite which acted as a conduit for oil in subsurface sections, e) Two sets of fractures in Upper Sarvak Fm. The wider set is completely filled with calcite cement and the second set is deprived of any cement and filled with blue dye, e) Compaction-associated fine crystalline dolomite replacing the calcite matrix

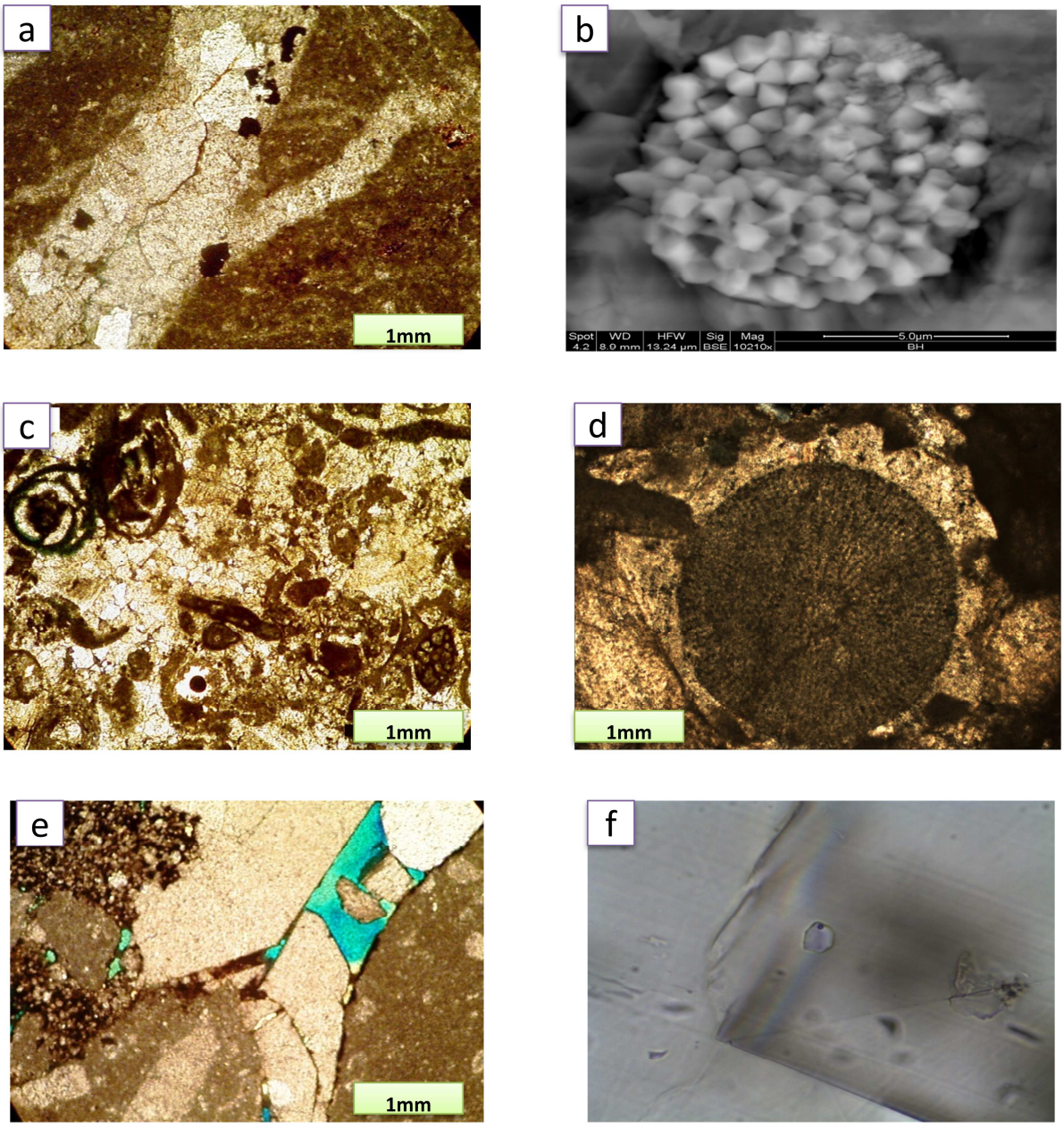

Figure 4. a) Photomicrograph of pyrite crystals formed adjacent to blocky calcite cement in a vein, b) SEM picture of framboidal pyrite, c) Photomicrograph of equant calcite cement in a grainstone, d) Syntaxial overgrowth cement surrounding an Echinoderm in a grainstone, e) Blocky calcite cement and intercrystalline porosity filled with blue dye, f) Photomicrograph of two- phase fluid inclusion in blocky calcite cement (magnification x100)

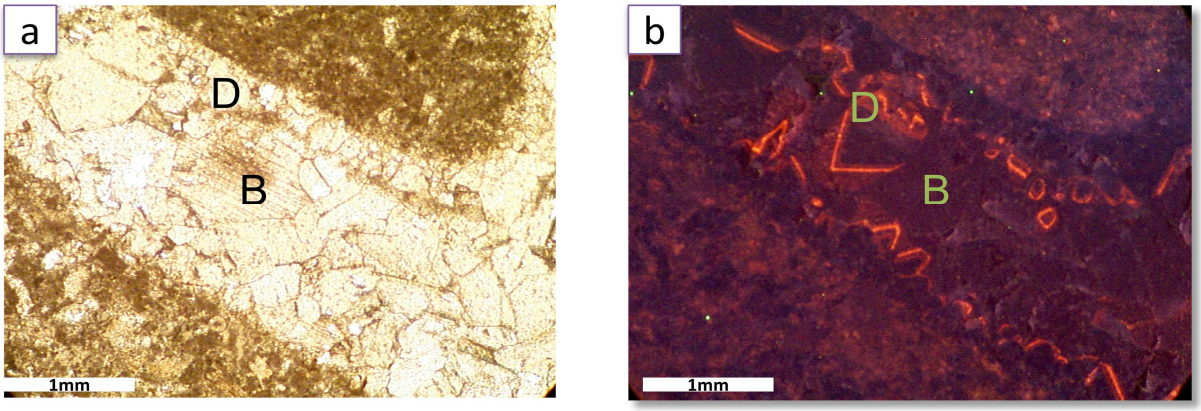

Figure 6 a) Drusy (D) and Blocky (B) calcite cement cements filling a moldic porosity, b) the same view of those cements under CL showing bright rims of drusy calcite cement and dark/non luminescent blocky calcite cement

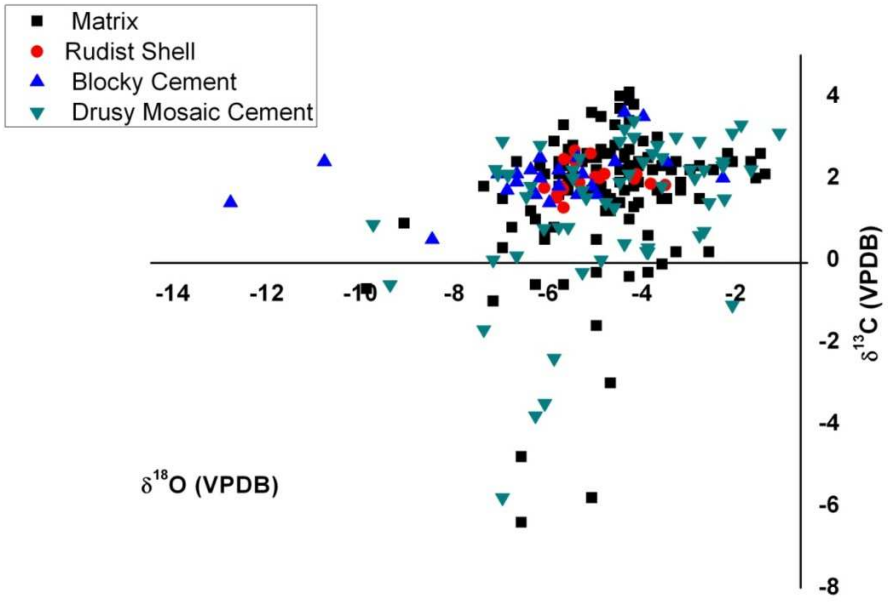

Figure 7. Plot of carbon and oxygen isotopic data of all carbonate components of the Sarvak Formation. The isotopic values of most of the samples fall within the Cenomanian-Turonian calcite range defined by Veizer et al., 1999

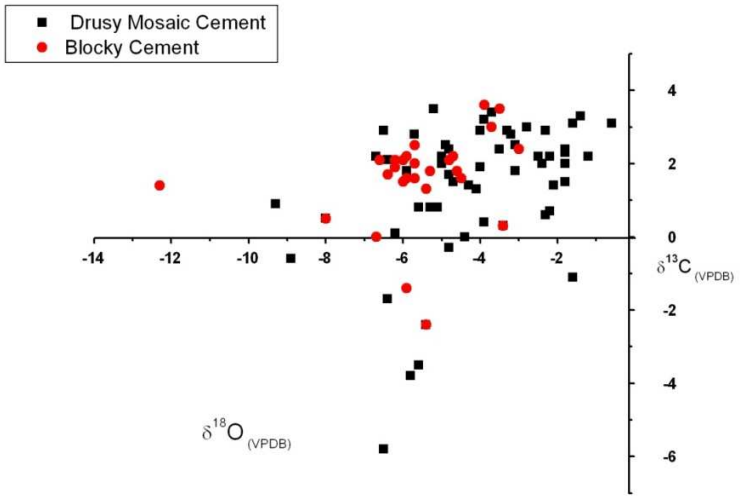

Figure 8 Carbon and oxygen isotopic composition of drusy mosaic and blocky calcite cement of the Sarvak Formation in the study area showing some overlap of isotopic values that could imply their precipitation from fluids of the same origin.

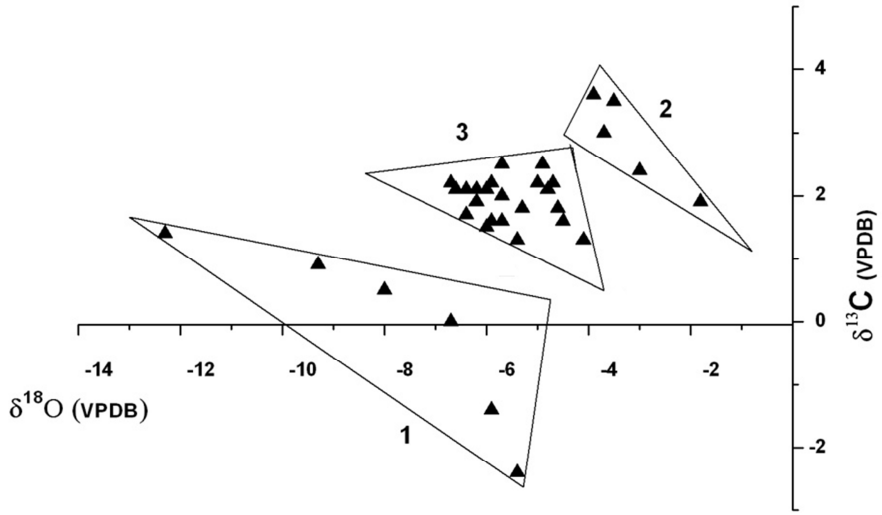

Figure 9 Carbon and oxygen isotopic composition of blocky calcite cement of the Sarvak Formation showing three distinct groups implying their precipitation from fluids of different origin.

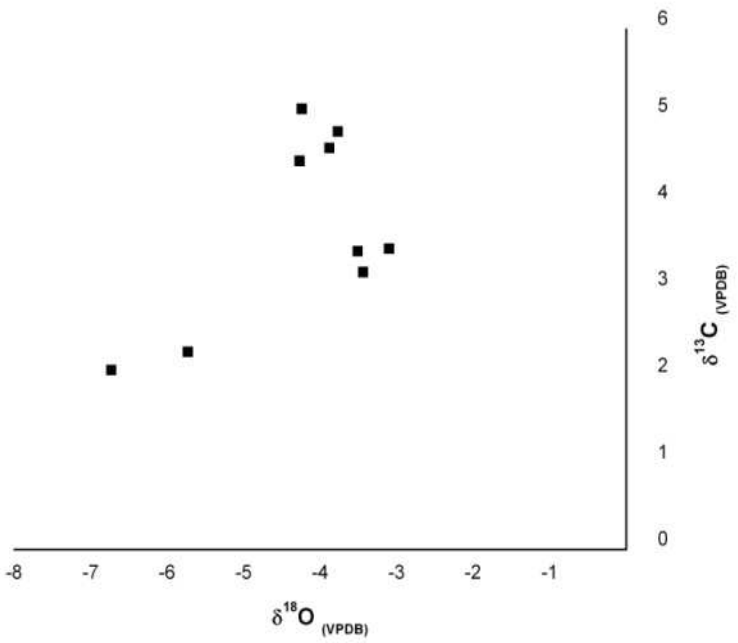

Figure 10 Carbon and oxygen isotope data of the compaction-related dolomite in the Upper Sarvak Formation

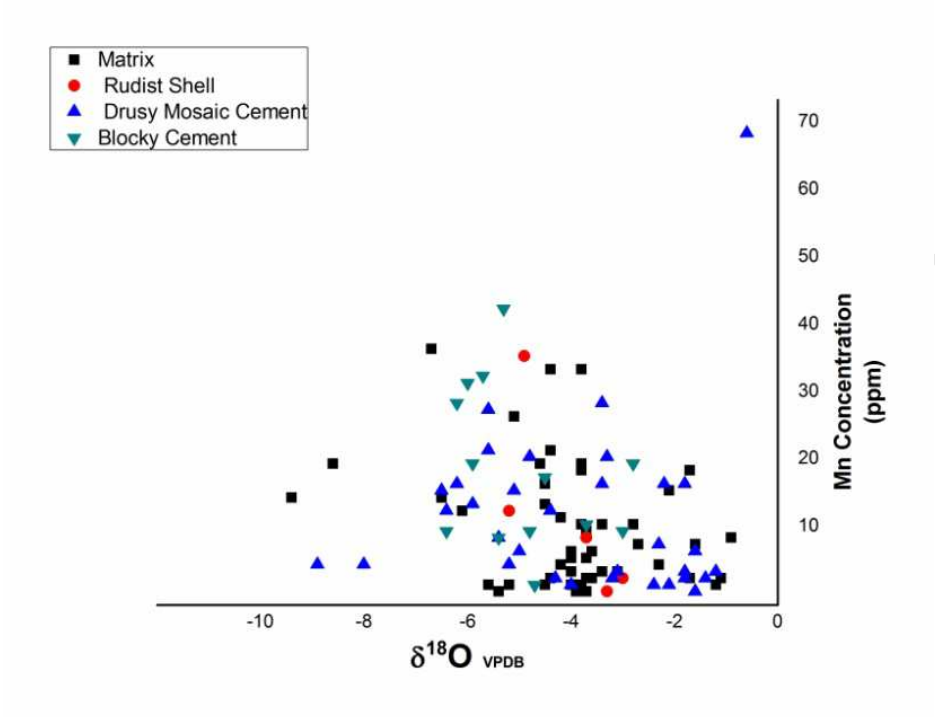

Figure 11. Plot of stable oxygen isotope values vs. manganese of the all carbonate component of the Sarvak Formation. Lack of distinct trend in carbonate matrix samples confirms that this marine carbonates have not been altered

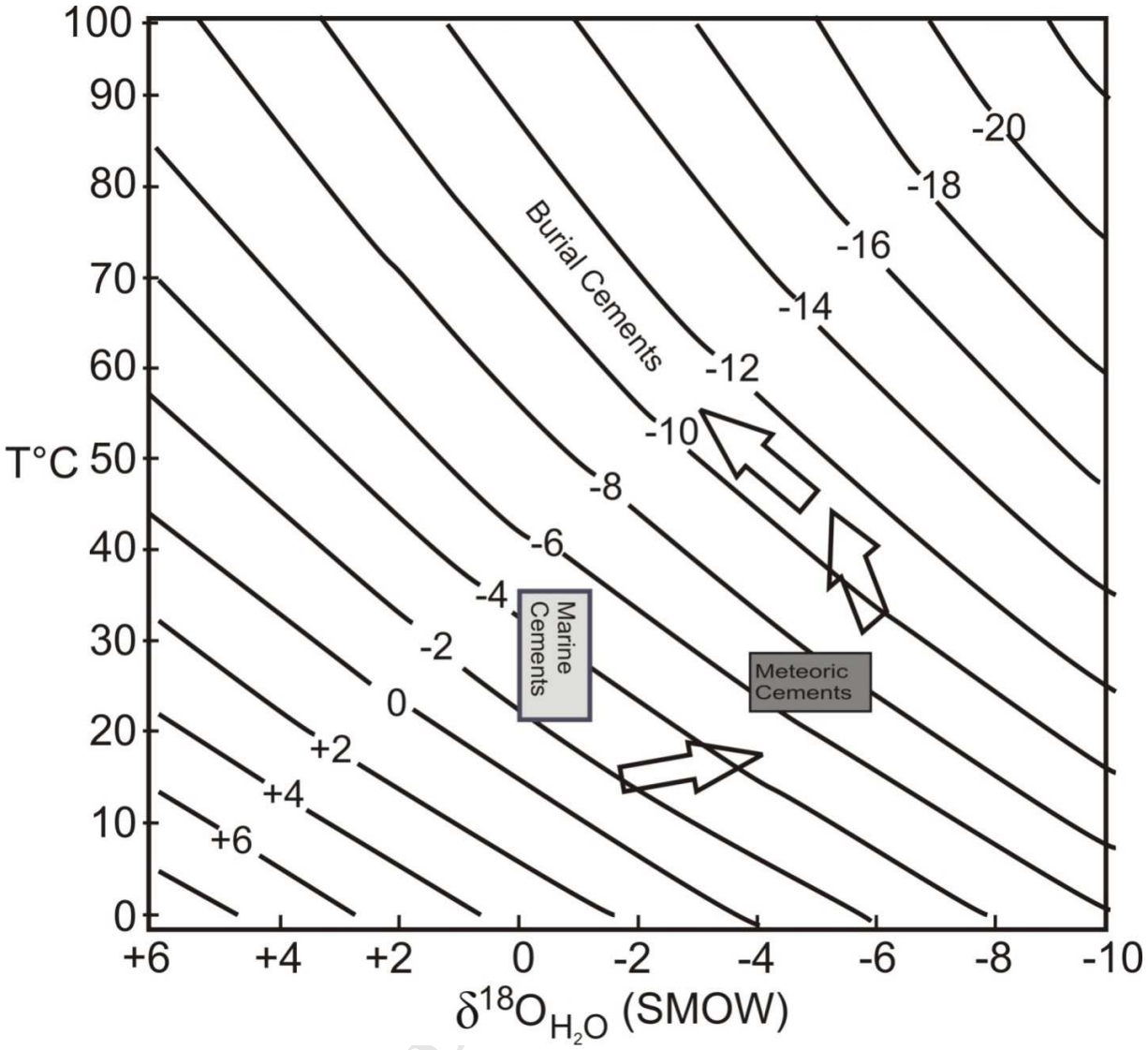

Figure 12. History of calcite cementation. The earliest cement precipitated from marine water with $\delta^{18}O$ ranging from -1.2 to 0‰. The shift in $\delta^{18}O$ indicated by the arrow is interpreted as an effect of changes in isotopic composition of the pore water from marine to dominantly meteoric water ($\delta^{18}O$ = -6±1‰) causing precipitation of some of the ^{18}O-depleted calcite cement (dark grey box). The most ^{18}O-depleted cement precipitated from heated mixed meteoric-marine waters.

As requested the followings are the five important items which I think are the major contribution to the geology of the Sarvak Formation;

1. For the first time, the diagenetic history of the Upper Sarvak Formation as the second most important oil reservoir in southern Iran has been studied in detail.
2. All aspects of diagenesis of the formation have been described and the mechanisms responsible for their formation have been explained.
3. The effects of diagenesis on the reservoir characteristics are determined.
4. Geochemical tools have been effectively applied to demonstrate the digenetic processes.
5. Diagenetic processes and products investigated and correlated in a vast oil producing region in outcrops and subsurface equivalents.